1 **Levee breach-induced compound flood modeling in Qianbujing Creek, Shanghai**

2 **during Typhoon "Fitow"**

3

4 Yuhan Yang[1], Jie Yin[2, 3, 4*], Weiguo Zhang[1], Yan Zhang[2], Yi Lu[2], Aoyue Xiao[2], Yunxiao Wang[2],

5 Wenming Song[2]

6

7 1 State Key Laboratory of Estuarine and Coastal Research, East China Normal University, China

8 2 Key Laboratory of Geographic Information Science (Ministry of Education), East China Normal

9 University, China

10 3 Department of Civil and Environmental Engineering, Princeton University, USA

11 4 Institute of Eco-Chongming, East China Normal University, China

12 * Correspondence to: J.Y. (email: jyin@geo.ecnu.edu.cn)

13

15

16 **Abstract:** Levee breach-induced flooding occurs occasionally but always causes considerable

17 losses. A serious flood event occurred due to the collapse of a 15-m-long levee section in

18 Qianbujing Creek, Shanghai, China, during typhoon "Fitow" in Oct 2013. Heavy rainfall

19 associated with the typhoon intensified the flood severity (extent and depth). This study

20 investigates the flood evolution to understand the dynamic nature of flooding and the compound

21 effect using a well-established 2D hydro-inundation model (Floodmap) to reconstruct this

22 typical event. This model coupled urban hydrological processes with flood inundation for high-

resolution flood modeling, which has been applied in a number of different environments, and

Floodmap is now the mainstream numerical simulation model used for flood scenarios. Our

simulation results provide a comprehensive view of the spatial patterns of the flood evolution.

The worst-hit areas are predicted to be low-lying settlements and farmland. Temporal

evaluations suggest that the most critical time for flooding prevention is in the early 1~3 hours

after dike failure. In low-elevation areas, temporary drainage measures and flood defenses are

equally important. The validation of the model demonstrates the reliability of the approach.

Key words: levee breach; compound flooding; inundation modeling; Shanghai

1. Introduction

Flooding is a common and devastating natural hazard, causing considerable personal injury, loss of life, and property damage worldwide (Jonkman et al., 2005; Jongman et al., 2012). Engineering measures such as dikes and barriers are typically constructed in low-lying deltas and floodplains to prevent flooding. However, weak or aging dikes without regular maintenance may fail during extreme flood events. Levee breaches may result in extensive flooding and damages throughout the hinterland (Ying et al., 2003). For example, Hurricane Katrina-induced flooding significantly damaged the dike system of New Orleans and overwhelmed the city, making it the costliest disaster in U.S. history (Kates et al., 2006). A more recent flood catastrophe with more than 50 deaths and hundreds of missing people resulted from a dam breach due to a Himalayan glacier outburst flood in northern India (Devjyot Ghoshal et.al, 2021).

In addition, riverine or storm-induced flooding is typically associated with heavy precipitation. The compound effect of pluvial, fluvial, or coastal flooding is much greater than the effect of individual flood events (Wahl et al., 2015). For instance, typhoon "Fitow" in 2013 brought torrential rain and caused high storm surges, resulting in record-breaking riverine water levels in the upstream region of the Huangpu River, Shanghai, China. As a result, the floodwall along the upstream Qianbujing Creek could not withstand the high water level, leading to a breach in a 15-m long section at 14:30 on 8 Oct 2013. Although the broken section was repaired after about 8 hours, the levee breach combined with heavy precipitation resulted in extensive flood

67   inundation in the rural areas.

68

69   Over the last few decades, dike failure-induced flooding and the compound effect have received

70   increasing attention from decision-makers, researchers, and even the general public. Recent

71   studies have provided considerable progress on dike reliability analysis and compound flood

72   modeling (Curran et al., 2018; Naulin et al., 2018). Several approaches for levee breach-induced

73   flood modeling were developed. Some previous studies have investigated the breaching

74   mechanism and the hydrological process of dike failure flooding, Vorogushyn (2010) proposed

75   an Inundation Hazard Assessment Model (IHAM), which coupled a 1D hydrodynamic model

76   of river channel routing, a probabilistic dike breach model, and a 2D raster-based inundation

77   model. Cannata et al. (2011) used a GIS-based approach to simplify a 2D dam break simulation.

78   Recent advances have been made in the application of methodologies for predicting the dike failure-

79   induced flooding, Yin et al. (2020) predicted dike failures and flood inundations in Shanghai,

80   China, under various emission scenarios using an interdisciplinary process-based approach.

81

82   Similarly, numerous studies analyzed the compound effects of various flood hazards at different

83   scales (Ganguli et al., 2020). Most previous studies focus on calculating the joint flood risk

84   probability. For instance, Lian et al (2013) evaluated the joint probability of rainfall and tidal

85   level both exceeding their threshold values through the copula and then analyzed the combined

86   effect of them on flood risk in a complex river network in a coastal city in China. At a global

87   scale, Couasnon (2020) and Eilander (2020) explored the compound flood potential resulting

88   from storm surges and riverine floods.

89

90   The above studies contributed significantly to the modeling and evaluation of dike failure-

91   induced flooding, as well as compound flood risk. However, few studies investigated the

92   compound influences of pluvial and levee breach-induced flooding or focused on the dynamic

93   process and mechanism of these cases, which can guide the development of appropriate

94   emergency response plans. Moreover, real-life cases of historical flooding events have not been

95   adequately investigated but can demonstrate the feasibility and robustness of the model. To

96   address the research gaps, this case study seeks to examine the changing nature of levee breach-

97   induced compound flooding. A simple 2D hydro-inundation model Floodmap is used to

98   simulate the process of the compound flood event that occurred in Qianbujing Creek to improve

99   our understanding of the evolution of flood inundation. The results of the approach are validated

100 by field measurements, including the inundation depth and the flood extent over time. The

101 findings can provide support for decision-makers to develop flood adaptation measures.

102

103 **2.   Materials and methods**

104

105 **2.1 Study area**

106

107 The study area is located at the junction of the Huangpu River and Qianbujing Creek in the

108 upstream Huangpu River Basin, Shanghai, China. The rural area covers about 1.5 km^2 with the

109 majority being agricultural land and the minority being human settlements. It is characterized

110 by a mild and low-lying topography (with an average altitude of about 3 m above Wusong

111   Datum). Due to its location, the study area has faced high flood risk from the river system;

112   however, the heights of the flood defense measures are relatively low (i.e., a 50-year return

113   period flood protection standard) compared to the high floodwall (1000-year period flood

114   protection standard) along the middle and downstream urban regions of the Huangpu River

115   (Yin et al., 2020). Furthermore, because of the northern subtropical monsoon climate in this

116   region, pluvial flood events caused by extreme rainfall, typically associated with typhoons, are

117   frequently recorded during the flood season (June to September) (Yin & Zhang, 2015).

118   Therefore, the risk of compound flooding from both riverine and pluvial sources is significantly

119   higher than that in other locations. Figure 1 shows the location of the study area and the levee

120   breach during typhoon "Fitow".

121

122   **2.2 Data sources and processing**

123

124   **2.2.1   Topographic data**

125

126   We used a 6-m resolution digital surface model (DSM) of the study area constructed from

127   images of the China Resource 3 satellite (ZY-3) and other high-resolution satellites. Since

128   buildings and trees represent barriers to water flow and reduce the area available for water

129   storage in the hydrodynamic model, we removed the non-topographic features (e.g., trees and

130   buildings) according to the Google historical dataset of remote sensing images to generate a

131   bare-earth digital elevation model (DEM) based on the Wusong Datum of Shanghai. (Fewtrell

132   et al., 2010; Neal et al., 2011; Yu & Lane, 2006b). We further resampled the cell size of the

133 bare-earth DEM from 6 m to 2 m using ArcGIS software to improve the spatial resolution of

134 the flood inundation model. The simulation domain of the study area consisted of 0.3 million

135 cells with an area of nearly 1.26 km^2.

136

137 **2.2.2   Precipitation and water level**

138

139 Time series of the precipitation and water level records during Typhoon "Fitow" were used as

140 boundary conditions to simulate the hydrodynamic process of the levee breach-induced

141 flooding and the rainfall-runoff. The data are typically derived from the stage measurements at

142 gauge stations or radar-based rainfall data. However, due to the small scale of the study area,

143 the gauging records are considered to be more reliable. Thus, we collected the historical records

144 of the precipitation and water level data at the nearest gauging station from 0:00 on 8 Oct to

145 12:00 on 9 Oct 2013 for about 12 hours before and after the levee failure.

146

147 The station-based precipitation records (at one-hour intervals) were obtained from the

148 Information Center of the Shanghai Meteorological Administration. The water level data (at 5

149 min intervals) at the closest gauging station along the Huangpu River (i.e. Songpu Bridge

150 gauging station at the upstream of the Huangpu River, about 4 km away from Qianbujing Creek)

151 were provided by the Shanghai Municipal Water Administration. The time series of the rainfall

152 and water level data interpolated from the gauging stations is shown in Figure 2. Heavy rainfall

153 occurred four hours before the levee breach, with the maximum hourly rainfall exceeding 20

154 mm/h, resulting in the high water level of the river. Due to the high rainfall and rising storm

tide, the water level increased rapidly to nearly 4.8-m and caused the collapse of a 15-m long

floodwall section at about 14:30 on 8 Oct.

2.2.3 Validation data

Aerial images or field surveys of flood extent were not available for the study event. There was

also a lack of water depth data from electronic gauges and flood incidents reported by the public.

Therefore, we validated the model through the field investigation of high watermarks in the

study area. We visited the study area three times in 2020 and investigated the residential areas

(house by house), roadways, and farmland mostly affected by the flood event. Validation data

were collected using questionnaires, and the coordinates of the locations were recorded by GPS.

However, since this flood event occurred more than 7 years ago, there are inherent uncertainties

in the investigation due to the changing environment and people's fading memory for the details

of the event. Similarly, people tend to exaggerate their injuries and losses during hazards; thus,

questionnaires can be highly biased. Finally, we pinpointed 32 incidents in total where locations

are confidently identified. Among the 32 observed inundation data, 14 were buildings, 10 were

roadways, and 8 were farmland locations (Figure 3).

2.3 Levee breach modeling

In general, levee breach mechanisms mainly include structural instability failures and structural

strength failures. The former pattern includes horizontal instability and rotational instability,

177   whereas the latter refers to the destruction of structures (Wang, 2016). Due to the configuration

178   of the floodwalls and the soil structure in Shanghai, structural instability failures always occur

179   during low water levels when critical inundation is less likely. In this case, structural strength

180   failure was considered the major reason for the levee breach in the study area, namely, the levee

181   collapse under an excessive hydraulic load on the wall due to an extremely high water level or

182   the uneven settlement of the floodwalls.

183

184   We identified the location of the levee breach from the historical news reports and through field

185   investigation. The 15-m long levee breach was located at the junction of Qianbujing creek and

186   the main channel of the Huangpu River. The levee height and location were obtained from the

187   Shanghai Municipal Institute of Surveying and Mapping. The height of the remaining intact

188   floodwalls without the breach section (about 5 m above Wusong Datum) was then overlaid onto

189   the original bare-earth DEM using the raster calculator in ArcGIS 10.6 software.

190

191   **2.4 Compound flood modeling**

192

193   The compound flood modeling was performed using a 2D hydro-inundation model (FloodMap)

194   (Yu & Coulthard, 2015; Yu & Lane, 2006a; 2006b), which couples hydrological processes (e.g.,

195   infiltration, evapotranspiration, and drainage) module with 2D surface flood inundation

196   modeling. The Floodmap model provides an effective approach for compound flood simulation,

197   allowing for more than one hydrological boundary condition, including pluvial, fluvial, coastal,

198   and groundwater sources. In this study, the compound effect of pluvial and fluvial flooding was

199 investigated. The fluvial flood modeling and pluvial flood modeling are described in Sections

200 2.4.1 and 2.4.2, respectively.

201

202 **2.4.1 Fluvial flood modeling**

203

204 For simulating the levee breach-induced flooding, a simplified flood inundation module based

205 on a raster environment was used to solve the inertial form of the 2D shallow water equations.

206 The module considered the mass and momentum exchange between the river flow and

207 floodplain inundation, it has been used to simulate the dynamic nature of flood routing and to

208 extract potential flood maps (Yang et al., 2020; Yin et al., 2015). The 2D inundation model is

209 similar to the inertial algorithm of Bates et al. (2010). The difference is the time-step calculation

210 approach. The optimal time step is calculated using the subsequent iteration instead of using

211 the time step of the next iteration calculated by the current iteration. The main structure of the

212 model is presented below.

213

214 The Saint-Venant momentum equation without the convective acceleration has the following

215 form:

216
$$\frac{\partial q}{\partial t} + \frac{gh\partial(h+z)}{\partial x} + \frac{gn^2q^2}{R^{4/3}h} = 0 \tag{1}$$

217 where g is the acceleration of gravity, q is the flow per unit width, R is the hydraulic radius,

218 h is the water depth, z is the bed elevation, and n is Manning's roughness coefficient. For

219 wide and shallow flows, R can be approximated with h. The equation discretized with respect

220 to time is:

$$221 \qquad \frac{q_{t+\Delta t}-q_t}{\Delta t} + \frac{gh_t\partial(h+z)}{\partial x} + \frac{gn^2 q_t^2}{h_t^{7/3}} = 0 \qquad (2)$$

222   The q_t in the friction term can be replaced by $q_{t+\Delta t}$ to obtain the explicit expression in the

223   next time step:

$$224 \qquad q_{t+\Delta t} = \frac{q_t - gh_t\Delta t\left(\frac{\partial(h_t+z)}{\partial x}\right)}{(1 + gh_t\Delta t n^2 q_t / h_t^{10/3})} \qquad (3)$$

225   The flows in the x- and y-directions are decoupled and have the same form. The discharge is

226   evaluated at the cell edges, and the depth is determined at the cell center. For model constancy

227   and minimizing numerical diffusion, we use the forward Courant-Friedrichs-Lewy condition

228   (FCFL), which was used by Yu & Lane (2011) for the diffusion-based version of FloodMap, to

229   calculate the time step in the inertial model:

$$230 \qquad \Delta t \le \min\left(\frac{wd_id_jn}{d_i^{1.67}(S_i)^{1/2} + d_j^{1.67}(S_j)^{1/2}}\right) \qquad (4)$$

231   where w represents the cell size, i and j are the indices for the flow direction in the x- and

232   y-directions, d_i and d_j are the effective water depths; S_i and S_j are the water surface

233   slopes. The effective water depth is defined as the difference between the high water surface

234   elevation and the high bed elevation of two cells that exchange water. The minimum time step

235   that satisfies the FCFL condition for all wet cells is used as the global time step for this iteration.

236   This approach does not require the back-calculation of the Courant number because the time

237   step is calculated based on the CFL condition that satisfies every wet grid cell for the current

238   iteration. The universal time step calculated with the FCFL may need to be scaled further by a

239   coefficient with a value between 0 and 1 because the FCFL condition is not strictly the right

240   stability criteria for an inertial system. A scaling factor in the range of 0.5–0.8 was found to

241   yield a stable solution in previous studies; here, a scaling factor of 0.7 was used for all

242   simulations. The calibration and validation of the model for the study area were conducted by

243   Yin et al. (2016).

244

245   **2.4.2   Pluvial flood modeling**

246

247   In terms of the pluvial flooding module, we ran the surface water flood routing using the same

248   structure as the fluvial flooding module. The infiltration over saturation was calculated by the

249   widely used Green-Ampt equation, and the evapotranspiration was represented using a simple

250   seasonal sine curve of daily potential evapotranspiration (Calder et al., 1983). This module also

251   considered the amount of runoff loss to the urban storm sewer systems by scaling the drainage

252   capacity (mm/h) for each time step.

253

254   The infiltration over saturation was determined by the widely used Green–Ampt equation,

255   which approximates the rate of infiltration as a function of the capillary potential, porosity,

256   hydraulic conductivity, and time using the following form:

257 $$f(t) = K_s \left(\frac{\varphi_f + h_o}{z_f} + 1 \right) \tag{5}$$

258   where K_s expresses the hydraulic conductivity of the saturated soil, φ_f is the capillary

259   potential across the wetting front, h_o is the water ponding on the soil surface, and z_f is the

260   cumulative depth of infiltration.

261

262   The evapotranspiration was determined using a simple seasonal sine curve of daily potential

263   evapotranspiration (Calder et al., 1983) as follows:

264 $$E_p = \overline{E_p} \left[1 + \sin\left(\frac{360i}{365} - 90 \right) \right] \tag{6}$$

265   where E_p is the mean daily potential evapotranspiration, and i is the day of the year. The

266   mass lost to evapotranspiration is typically limited due to the short duration of urban pluvial

267   flooding.

268

269   We used the topography boundary conditions, flow boundary conditions, and precipitation

270   boundary conditions as inputs to model a 36-h compound flood process, including the 12 h

271   before and after the levee breach, and we assumed evapotranspiration of 3 mm/day, a value that

272   which generates a good inundation prediction in the urbanized area (Yin et al., 2016; Yu and

273   Coulthard, 2015). The soil hydraulic conductivity (K_s) is an important but highly complex

274   parameter used to calculate infiltration. Empirically-based correlation methods or in situ

275   hydraulic laboratory measurements can be used to determine the value of K_s. Given the

276   practical constraints, this study refers to previous flood simulations in Shanghai (Yin et al.,

277   2016; Yin et al., 2015; Yu & Coulthard, 2015; Yu et al., 2016) and used the value of 0.001 m/h

278   for the hydraulic conductivity. A relatively high roughness value (n = 0.06) was used in the

279   simulation, according to the type of cultivated land and crops in the study area. Since the

280   Qianbujing creek is located in a rural area, we did not consider the urban storm drainage

281   capacity in this simulation.

282

283   **3.   Results**

284   **3.1 Time series of flood inundation**

285

286   Figure 4 shows the changes in the predicted flood inundation every 4 h during the event, and

287   Figure 5 depicts the time series of average water depth and flood extent. These results show the

288   spatial and temporal evolution of the levee breach-induced compound flooding during typhoon

289   "Fitow". Prior to the levee breach, it is apparent from Figures 4 and 5 that heavy rainfall in the

290   study area led to localized shallow waterlogging, mainly in the low-lying farmland and forests.

291   The inundation area reached its first peak in the early hours on 8 Oct, but the water retention

292   time was very short due to the shallow water depth (< 15 cm). At around 11:00 am on 8 Oct,

293   another short-term rainstorm with rainfall over 20 mm/h occurred. Shortly after the

294   precipitation peak, the water level of Qianbujing Creek showed an increasing trend. The

295   compound effects of tide rising and heavy rain made the water level soon reached nearly 4.8 m

296   (Figure 2). Due to the high water pressure, the bearing capacity of the floodwall was exceeded,

297   resulting in a 15-m breached section (at 14:30). Subsequently, overland flow through breached

298   floodwalls and extensive flood inundation occurred quickly along the riverbank, first in the

299   low-lying farmland near the river and then on roads and residential areas. About 10 homes were

300   completely inundated during the water level rising period (until 16:00) with the maximum

301   inundation depth higher than 2 m. After 16:00, as the rainfall stopped and the water level

302   dropped, the inundation area gradually stopped spreading.

303

304   A cross-comparison of the derived flood hazard maps over time further indicated that although

305   the rainstorm caused extensive surface water flooding in the majority of the study area, the

306   inundation depth was generally shallow (< 15 cm). This effect can be attributed to the

307   evapotranspiration and infiltration in a few hours. However, unlike the short-term waterlogging

308   caused by the rainstorm, the compound effects of the rainfall and levee breach-induced flood

309   inundation continued over 12 h, with an average water depth of nearly 60 cm.

310

311   **3.2 Maximum flood inundation**

312

313   The maximum flood extent and inundation during the event are shown in Figure 6. We use 2

314   cm as the threshold for surface water flooding and treat water depths shallower than 2 cm as

315   sheet flow, which did not accumulate in topographic lows (Yu et al., 2016). Figure 6 shows that

316   over half (56%) of the study area was inundated from the compound flooding, and most of the

317   flooded areas were low-lying farmland with maximum flood depths of higher than 2 m. Aside

318   from the waterfront areas, many low-lying farmland areas were affected by the rainstorm, with

319   maximum water depths over 50 cm. In contrast, the water depth on the roads and the buildings

320   were shallow; most of it was less than 0.5 m and disappeared quickly. In nearly half of the

321   flooded locations, the water depths were between 2 cm and 15 cm (44.1%), and a smaller

322   proportion of the area (21.12%) had water depths between 15 cm to 50 cm. About 33.26% of

323   the inundated areas had water depths of 50 cm to 2 m. In combination with the time series of

324   water level and rainfall (Figure 2), It can be inferred that the maximum flood inundation

325   occurred at about the fourth hour after the levee breaching (at ~16:00) in the waterfront area,

326   while it occurred at about 11:30 a.m. in other areas.

327

328   **3.3 Model validation**

329

330   The field measurements were used to validate the performance of the compound flooding model.

331   Figure 6 shows the location of the measurement points. The points were divided into building,

332   road, and farmland types. Since there are few residential areas in the study area, reliable

333   inundation information could not be obtained in most flooding areas; therefore, most of the

334   points represent buildings with extensive inundation. Since there were uncertainties and errors

335   in the survey results, including the respondents' memory bias, exaggeration of inundation, and

336   false positives, we set the observed error to 5 cm for building points, 10 cm for road points, and

337   15 cm for farmland points. The simulation error was set as 5 cm. Figure 7 shows the scatter plot

338   of the simulated and observed water depth and the 95% confidence interval. A correlation was

339   observed between the simulated water depth and observed water depth, and most points fell

340   within the confidence band. The observed water depth was slightly higher than the simulated

341   water depth, which may be attributed to the exaggeration of the water depth by the respondents.

342

343   **3.4 Sensitivity analysis**

344

345   The model sensitivity to Manning's roughness coefficient over time was analyzed. Several

346   Manning's n values (0.01–0.1 at a 0.01 increment) were used for the roughness

347   parameterization. The difference between the average water depth (Figure 8a) and the total

348   inundation area (Figure 8b) predicted by the simulations with different n values was calculated

349   on a cell-by-cell basis. The results indicate similar trends of the average water depth and

350   inundation area for different roughness values and differences in the values. As the roughness

351   increased, the average water depth decreased, and the difference was more pronounced at higher

352   roughness values. For example, the maximum average depth decreased from 0.61 m to 0.55 m

353 with an increase in the n value of 0.01 to 0.1. Interestingly, there were differences in the

354 sensitivity to the roughness before and after the levee breach for the flood inundation extent.

355 The inundation area increased obviously as the roughness increased during the rainstorm, however,

356 it is decreased slightly with an increase in the n value during the levee breach when the river flooding

357 was the main force. The main reason which causes the sensitivity differences is the unlike formation

358 mechanism of inundation extent between rainstorm and fluvial flooding. These results demonstrate

359 the sensitivity of the model to the roughness.

360

361 **4. Conclusion and discussion**

362 Simulation of real-life historical severe flooding events can reveal the dynamic flooding process

363 and mechanism. In this study, a serious compound levee breach-induced flooding during the

364 typhoon "Fitow" has been adequately investigated used by a simple 2D hydro-inundation model

365 (Floodmap). The surface runoff caused by the rainstorm and river overflow was considered

366 well in the model.

367

368 The following conclusions can be drawn from the simulation results. First, one key advantage

369 of this modeling approach is the analysis of a single historic flood event. The flooding results

370 showed the time series of the flooding extent and inundation depth, indicating that the low-

371 lying area especially for farmland areas near the river had a very high flood risk. The compound

372 flooding caused extensive damage to low-lying areas not only due to the elevation but the lack

373 of a drainage network, resulting in an average water depth of over 0.5 m more than 12 h. Second,

374 within 1-3 h after the dike failure, the floodwaters spread rapidly, and the inundation area and

375 average water depth reached the peak value; chiefly because of the rising riverine tides at the same

376 time, however, during the falling tide period, although the dike has not been repaired, the flooding

377 diffusion tend to be slow, the flood risk decreased as the water level dropped as well. Thus, it

378 can be indicated that the levee breach-induced flooding spread was heavily dependent on the

379 change of riverine tides, the key period for levee breach-induced flooding control (such as

380 repairing the levee, evacuation) was from levee breach to the end of the rising tide. Third, the

381 water does not drain rapidly only by infiltration or evaporation, and the waterlogging lasted for

382 more than 12 h, resulting in loss of farmland with high vulnerability. Therefore, for levee

383 breach-induced flood response in the rural area, in addition to repairing the levee in time, it is

384 necessary to remove the flood water using drainage measures at the same time, such as setting

385 water pumps near the farmland or other low-lying area, when necessary, the government should

386 guide nearby residents to evacuate to a safe place as well.

387

388 Beyond the flood emergency response measures, effective long-term engineering measures may

389 be more suitable for fundamentally decreasing the unpredictable levee-breach flooding risk,

390 local specifications for flood-control engineering should be updated with the increasing flood

391 risk in the context of climate change (Yang et al., 2015).

392

393 Model validation was a challenging aspect of this research. The topographic data resolution,

394 land use, and land cover affect the simulation results. The validation data consisted of field

395 observations, and the uncertainty associated with incorrect recollections of the residents led to

396 errors. It was assumed that the error ranged from 5 cm to 15 cm for different land uses. Most

397 of the verification results matched the field observations and fell within the confidence band,

398 demonstrating the model's reliability. Nevertheless, some of the simulated water depths were

399 slightly smaller than the field observations, which was attributed to the exaggeration of the

400 depth by the respondents.

401

402 Another important component of this study is the comparison of the predictions (flooding extent

403 and average water depth) using different Manning's n values (from 0.01 to 0.1 at a 0.01 interval).

404 The results demonstrated the model's sensitivity to roughness. Overall, the model exhibited

405 good reliability for single and compound flood modeling. Future research on this topic should

406 be improved for the following aspects to improve the robustness of the model. (1) Higher-

407 resolution topography and hydrological boundary conditions should be used to represent typical

408 flood conditions. (2) The drainage capacity could be modeled to provide a more reliable result.

409 (3) Urban compound flood risks should be evaluated to help decision-makers develop effective

410 emergency response plans and flood adaptation strategies.

411

416

417 **Author contributions.** YY and JY initiated and led this research. YY designed the flood event
418 process, analyzed the performance of this model, and wrote the paper. JY provided history
419 records of water level. WZ and JY gave the suggestion for this paper. YL dealt with the rainfall
420 data. YZ, AX, YW and WS helped in collecting validation data.

Reference

Bates, P. D., Horritt, M. S., & Fewtrell, T. J. J. J. o. H. (2010). A simple inertial formulation of the shallow water equations for efficient two-dimensional flood inundation modelling. Journal of Hydrology, 387(1-2), 33-45.

Bevacqua, E., Maraun, D., Vousdoukas, M. I., Voukouvalas, E., & Widmann, M. J. S. A. (2019). Higher probability of compound flooding from precipitation and storm surge in Europe under anthropogenic climate change. Science Advances, 5(9), eaaw5531.

Calder, I. R., Harding, R. J., & Rosier, P. T. W. J. J. o. H. (1983). An objective assessment of soil-moisture deficit models. Journal of Hydrology, 60(1-4), 329-355.

Cannata, M., & Marzocchi, R. (2011). Two-dimensional dam break flooding simulation: a GIS-embedded approach. Natural Hazards, 61(3), 1143-1159.

Couasnon, A., Eilander, D., Muis, S., Veldkamp, T. I. E., Ward, P. J. J. N. H., & Sciences, E. S. (2020). Measuring compound flood potential from river discharge and storm surge extremes at the global scale. Natural Hazards and Earth System Sciences, 20(2), 489-504.

Curran, A., De Bruijn, K. M., & Kok, M. (2018). Influence of water level duration on dike breach triggering, focusing on system behaviour hazard analyses in lowland rivers. Georisk: Assessment and Management of Risk for Engineered Systems and Geohazards, 14(1), 26-40.

Devjyot Ghoshal., Manoj Kumar. (2021). Himalayan glacier breaks in India, around 125 missing in floods, https://www.reuters.com/article/us-india-disaster-idUSKBN2A706O

Eilander, D., Couasnon, A., Ikeuchi, H., Muis, S., Yamazaki, D., Winsemius, H. C., & Ward, P. J. J. E. R. L. (2020). The effect of surge on riverine flood hazard and impact in deltas globally. Environmental Research Letters, 15(10), 104007 (104012pp).

Fewtrell, T. J., Bates, P. D., Horritt, M., & Hunter, N. M. J. H. P. (2010). Evaluating the effect of scale in flood inundation modelling in urban environments. Hydrological Processes, 22(26), 5107-5118.

Ganguli, P., Paprotny, D., Hasan, M., Güntner, A., & Merz, B. (2020). Projected Changes in Compound Flood Hazard From Riverine and Coastal Floods in Northwestern Europe. Earth's Future, 8(11). doi:10.1029/2020ef001752

Jongman, B., Ward, P. J., & Aerts, J. C. J. H. (2012). Global exposure to river and coastal flooding: Long term trends and changes. Global Environmental Change, 22(4), 823-835. doi:10.1016/j.gloenvcha.2012.07.004

Jonkman, S. N. (2005). Global perspectives of loss of human life caused by floods. Natural Hazards, 34(2), 151-175.

Lian, J. J., Xu, K., Hydrology, C. M. J., Sciences, E. S., & Discussions. (2013). Joint impact of rainfall and tidal level on flood risk in a coastal city with a complex river network: a case study of Fuzhou City, China. Hydrology and Earth System Sciences, 17(1), 679-689.

Moftakhari, H. R., Salvadori, G., AghaKouchak, A., Sanders, B. F., & Matthew, R. A. (2017). Compounding effects of sea level rise and fluvial flooding. Proceedings of the National Academy of the Sciences of the United States of America, 114, 9785-9790.

Naulin, M., Kortenhaus, A., & Oumeraci, H. (2018). Reliability-Based Flood Defense Analysis in an Integrated Risk Assessment. Coastal Engineering Journal, 57(1), 1540005-1540001-1540005-1540035.

Neal, J., Schumann, G., Fewtrell, T., Budimir, M., Bates, P., & Mason, D. J. J. o. F. R. M.

469   (2011). Evaluating a new LISFLOOD-FP formulation with data from the summer 2007
470   floods in Tewkesbury, UK. Journal of Flood Risk Management, 4(2).

471 Vorogushyn, S., Merz, B., Lindenschmidt, K. E., & Apel, H. (2010). A new methodology for
472   flood hazard assessment considering dike breaches. Water Resources Research, 46(8).
473   doi:10.1029/2009wr008475

474 Wahl, T., Jain, S., Bender, J., Meyers, S. D., & Luther, M. E. (2015). Increasing risk of
475   compound flooding from storm surge and rainfall for major US cities. Nature Climate
476   Change, 5(12), 1093-1097.

477 Yang, L., Scheffran, J., Qin, H. et al. (2015) Climate-related flood risks and urban responses in
478   the Pearl River Delta, China. Regional Environmental Change, 15, 379–391.
479   https://doi.org/10.1007/s10113-014-0651-7

480 Yang, Y., Yin, J., Ye, M., She, D., & Yu, J. (2020). Multi-coverage optimal location model for
481   emergency medical service (EMS) facilities under various disaster scenarios: a case study
482   of urban fluvial floods in the Minhang district of Shanghai, China. Natural Hazards and
483   Earth System Sciences, 20(1), 181-195.

484 Yin, J., Jonkman, S., Lin, N., Yu, D., & Wang, J. J. E. s. F. (2020). Flood Risks in Sinking
485   Delta Cities: Time for a Reevaluation? Earth's Future, 8(8).

486 Yin, J., Yu, D., & Wilby, R. (2016). Modelling the impact of land subsidence on urban pluvial
487   flooding: A case study of downtown Shanghai, China. Science of the Total Environment,
488   544(July 2011), 744-753.

489 Yin, J., Yu, D., Yin, Z., Wang, J., Xu, S. J. L., & Planning, U. (2015). Modelling the
490   anthropogenic impacts on fluvial flood risks in a coastal mega-city: A scenario-based case
491   study in Shanghai, China. Landscape and Urban Planning, 136, 144-155.

492 Yin, J., & Zhang, Q. (2015). A comparison of statistical methods for benchmarking the
493   threshold of daily precipitation extremes in the Shanghai metropolitan area during 1981–
494   2010. Theoretical and Applied Climatology, 120(3-4), 601-607.

495 Ying, X., Wang, S. S. Y., & Khan, A. A. (2003). Numerical Simulation of Flood Inundation
496   due to Dam and Levee Breach. Paper presented at the World Water & Environmental
497   Resources Congress.

498 Yu, D., & Coulthard, T. J. J. J. o. H. (2015). Evaluating the importance of catchment
499   hydrological parameters for urban surface water flood modelling using a simple hydro-
500   inundation model. Journal of Hydrology, 524, 385-400.

501 Yu, D., & Lane, S. N. (2006a). Urban fluvial flood modelling using a two-dimensional
502   diffusion-wave treatment, part 1: Mesh resolution effects. Hydrological Processes, 20(7),
503   1541-1565.

504 Yu, D., & Lane, S. N. (2006b). Urban fluvial flood modelling using a two-dimensional
505   diffusion-wave treatment, part 2: Development of a sub-grid-scale treatment. Hydrological
506   Processes, 20(7), 1567-1583.

507 Yu, D., & Lane, S. N. (2011). Interactions between subgrid-scale resolution, feature
508   representation and grid-scale resolution in flood inundation modelling. Hydrological
509   Processes, 25(1), 36-53.

510 Yu, D., Yin, J., & Liu, M. (2016). Validating city-scale surface water flood modelling using
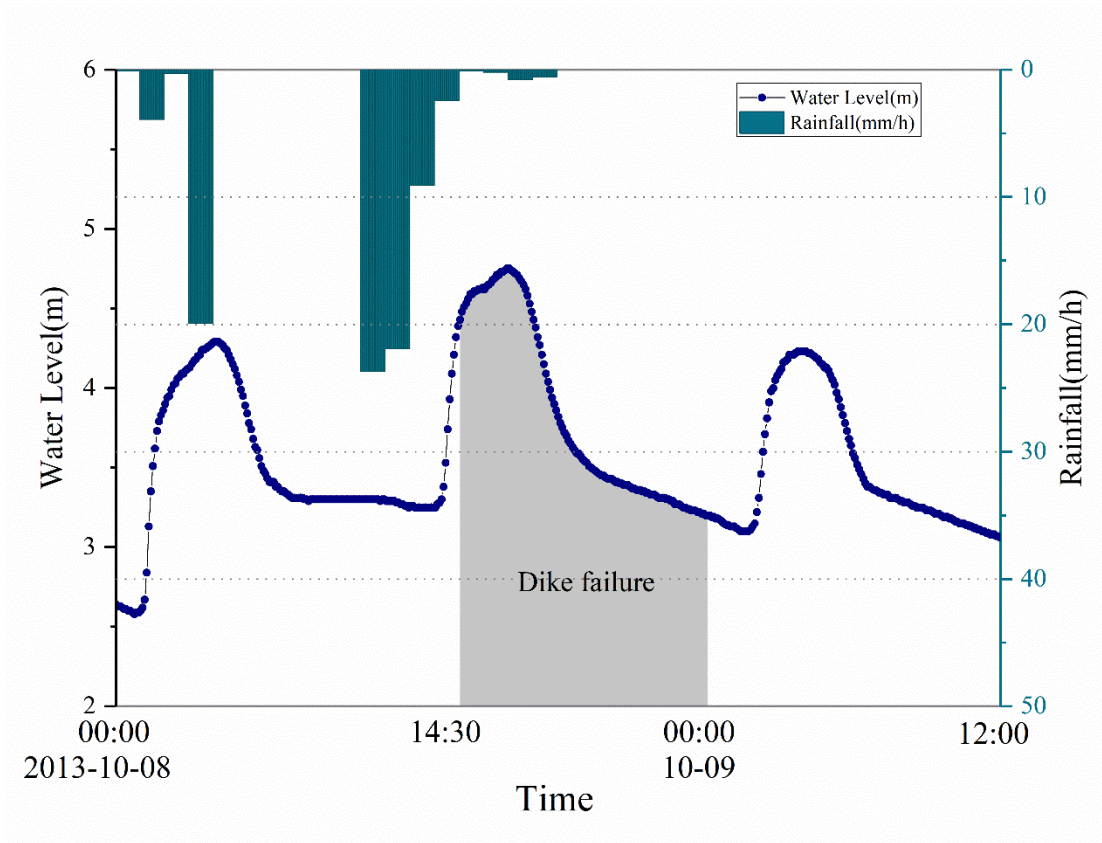511   crowd-sourced data. Environmental Research Letters, 11(12).

512
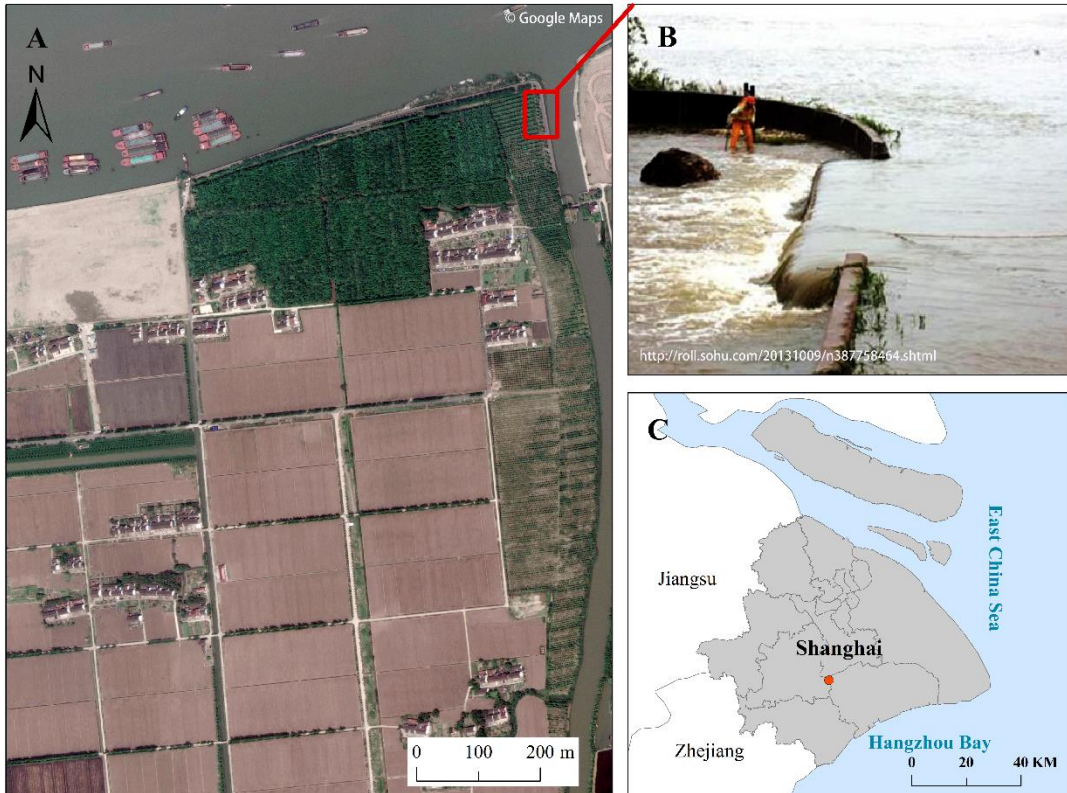
513

514   Fig. 1 Location of the study area and levee breach during typhoon "Fitow"

515

516   Fig.2 Time series of the water level and rainfall data at Qianbujing Creek during Typhoon

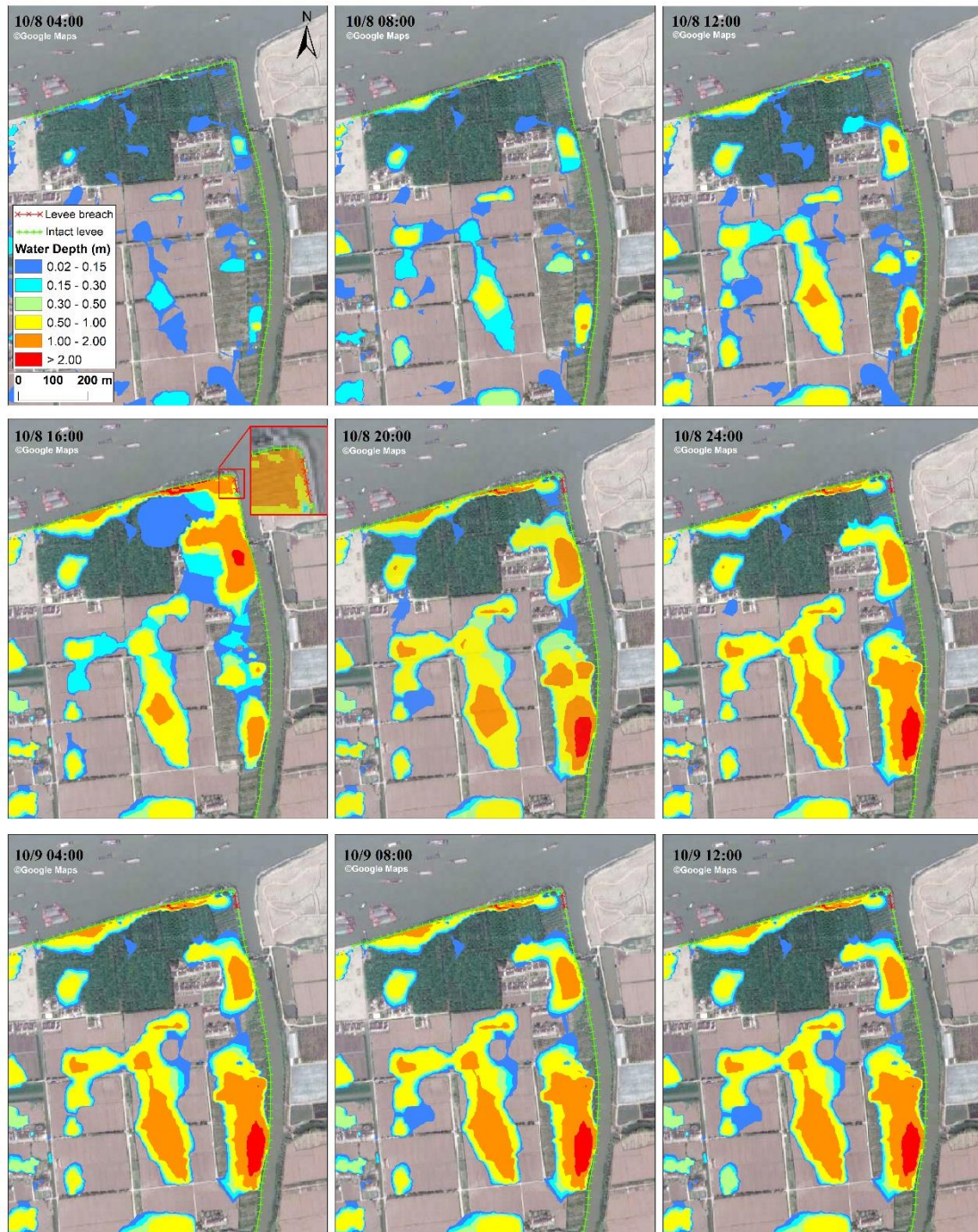517   "Fitow"

518

519

520

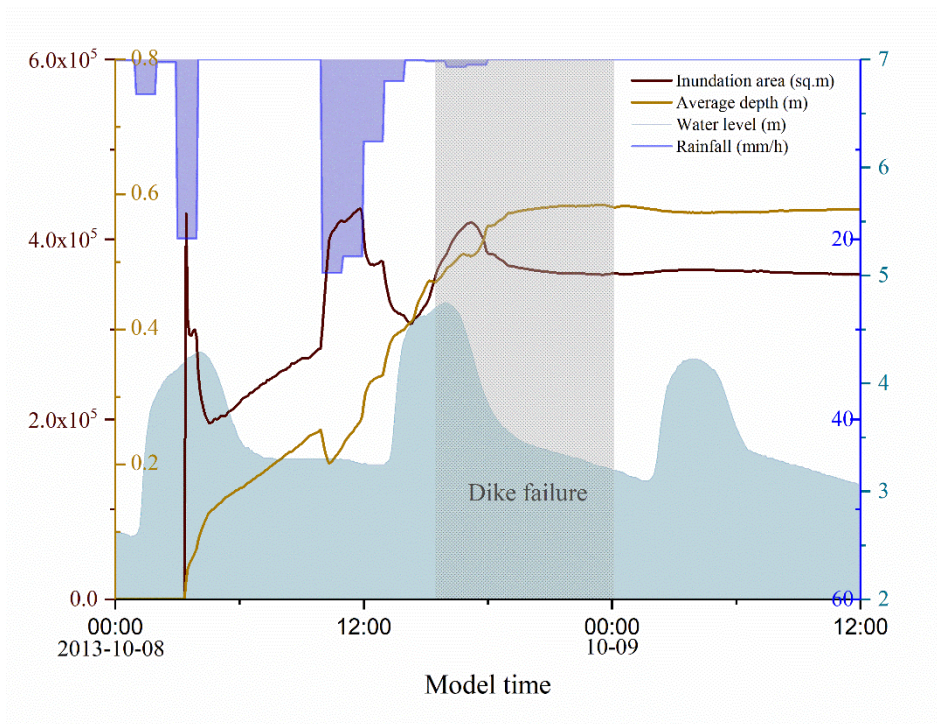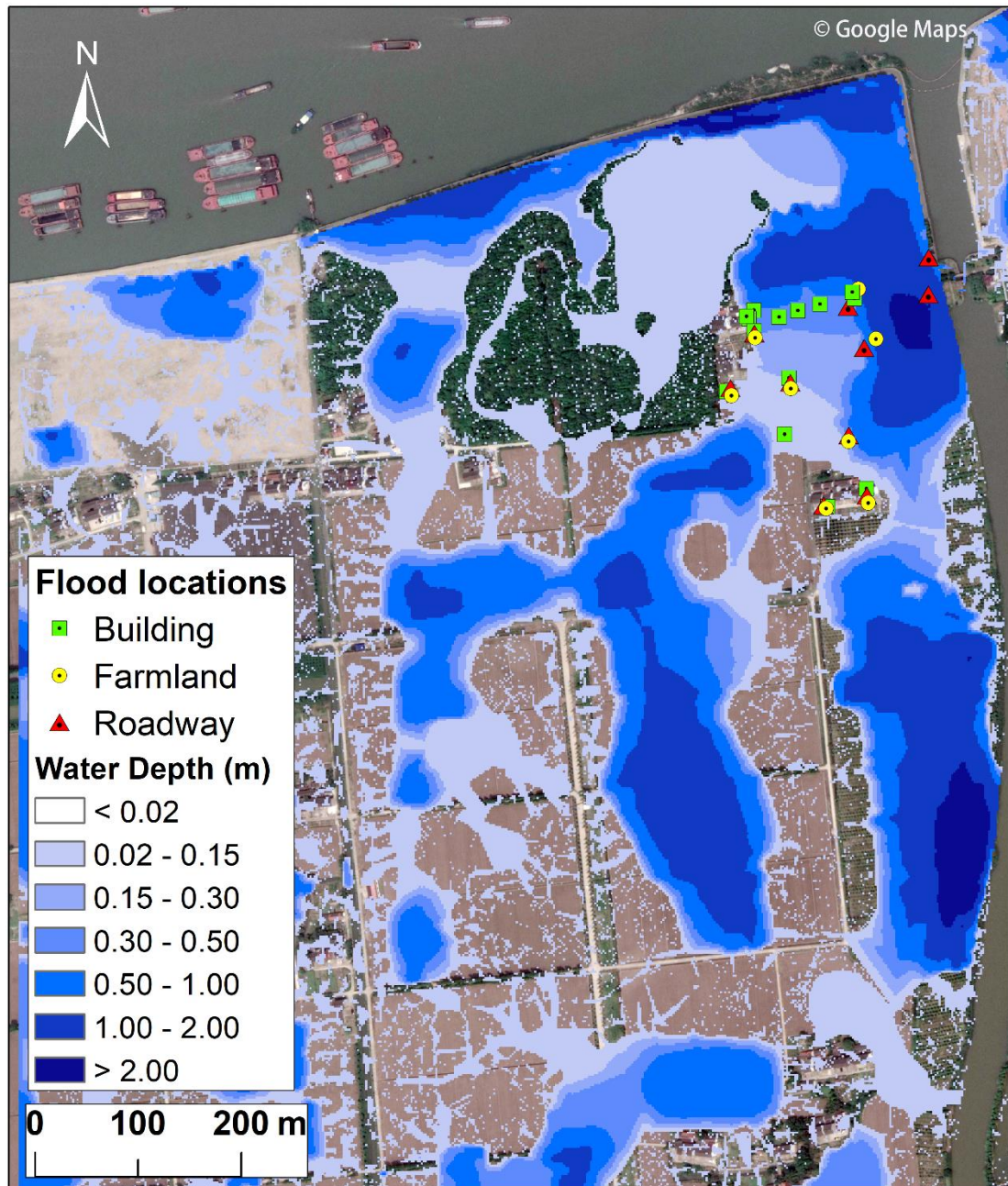521   Fig. 3 Field investigation of flood inundation after the event

Fig. 4 Time series of flood inundation during the typhoon event

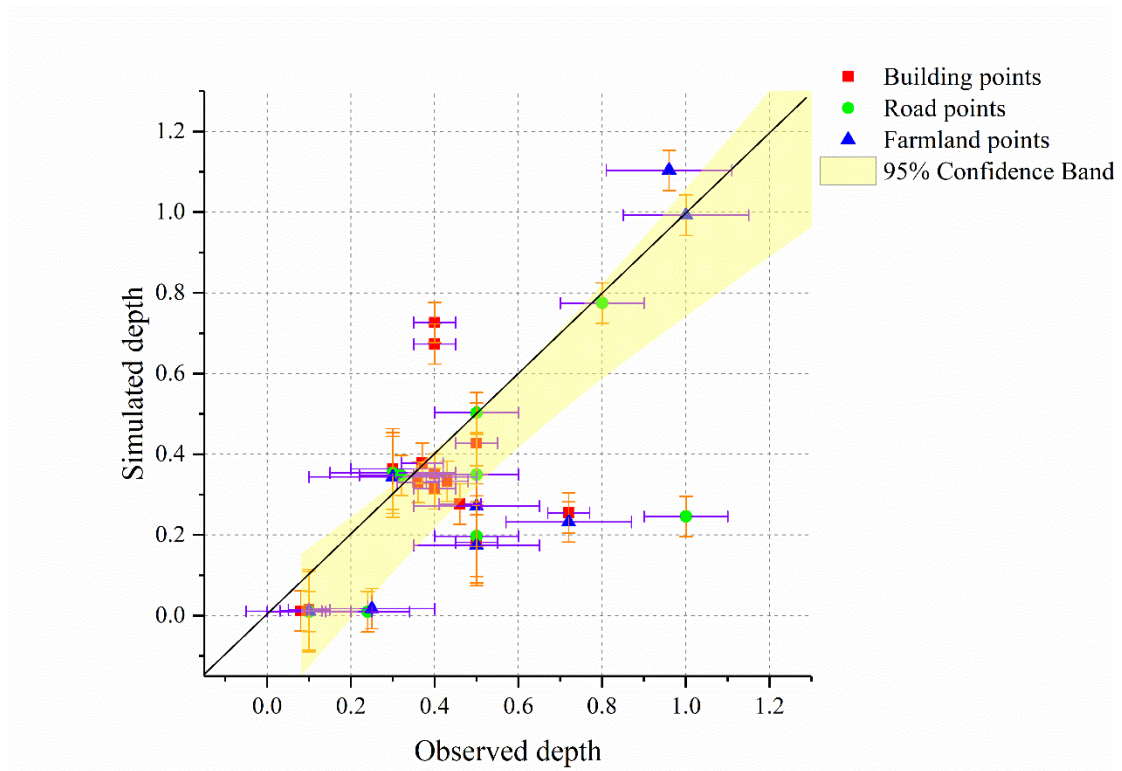Fig. 5 Time series of the inundation area and water depth during the flood event

524

525

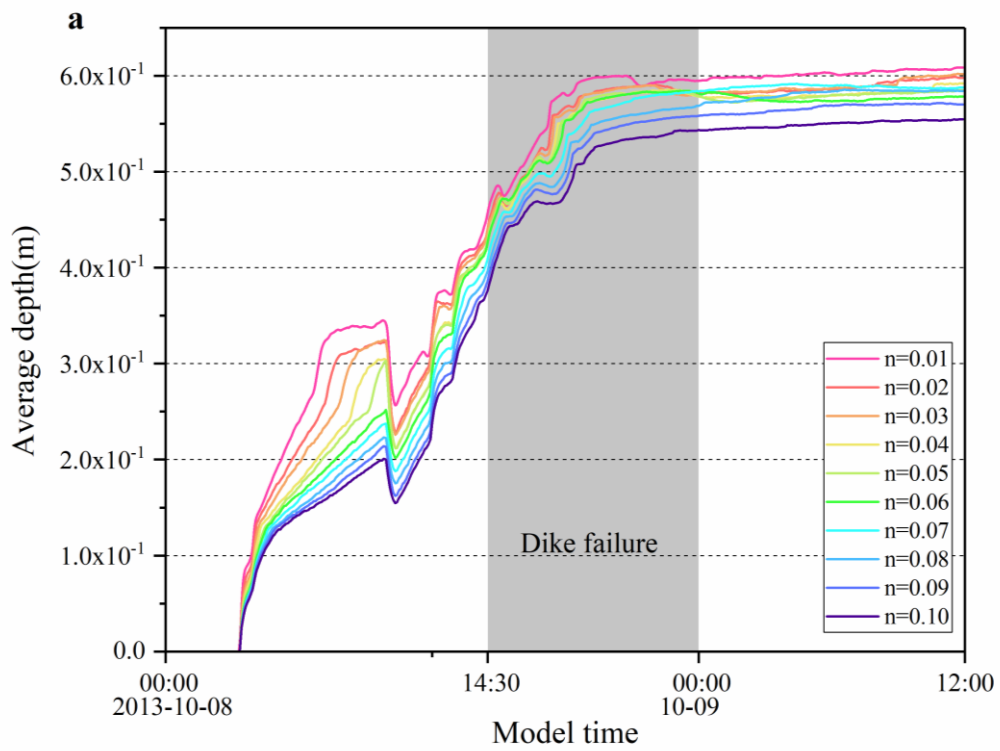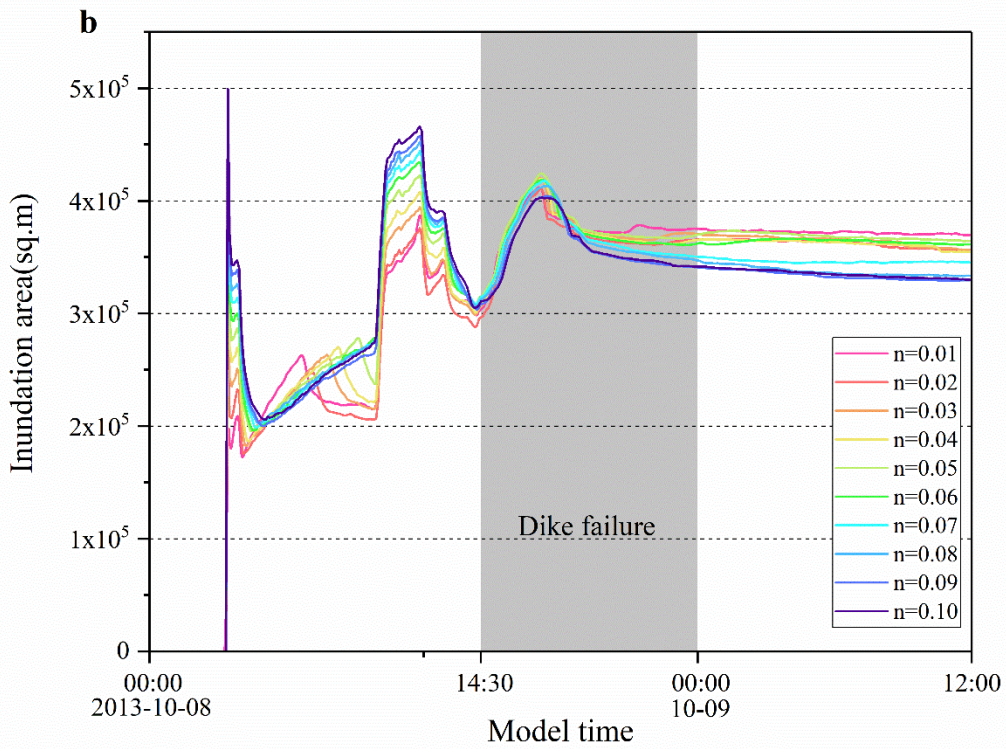527   Fig. 6 Maximum flood extent and depth predicted by the model

Fig. 7 A comparison of the simulated and observed depths

528

529

530

531

532

533

534   Fig. 8 Sensitivity analysis of the model to Manning's roughness coefficient